Extracellular vesicles produced by bone marrow mesenchymal stem cells attenuate renal fibrosis, in part by inhibiting the RhoA/ROCK pathway, in a UUO rat model

Zhengzhou Shi
Shanghai Children's Medical Center https://orcid.org/0000-0003-0014-9764
Qi Wang
Shanghai Children's Medical Center
Youbo Zhang
Nantong Maternal and Child Health Hospital
Dapeng Jiang (jdp509@163.com)

Research

Keywords: UUO, renal interstitial fibrosis, apoptosis, oxidative stress, MFG-E8, RhoA/ROCK

Posted Date: May 12th, 2020

DOI: https://doi.org/10.21203/rs.3.rs-17275/v2

Version of Record: A version of this preprint was published on June 26th, 2020. See the published version at https://doi.org/10.1186/s13287-020-01767-8.

Abstract

Background: Renal interstitial fibrosis is a critical symptom of chronic kidney disease that is associated with high incidence. Extracellular vesicles produced by bone marrow mesenchymal stem cells (BMSC-EVs) can play important roles in the repair of injured tissues. Though numerous studies have reported the effect of EVs on renal fibrosis, the underlying mechanisms remain unclear. We hypothesized that BMSC-EVs containing milk fat globule–epidermal growth factor–factor 8 (MFG-E8) could attenuate renal fibrosis by inhibiting the RhoA/ROCK pathway. Methods: We investigated whether BMSC-EVs have antifibrotic effects in a rat model of renal fibrosis, in which rats were subjected to unilateral ureteral obstruction (UUO), as well as in cultured HK2 cells. Extracellular vesicles from BMSCs were collected and co-cultured with HK2 cells during transforming growth factor-β1 (TGF-β1) treatment. HK2 cells co-cultured with TGF-β1 were also treated with the ROCK inhibitor, Y-27632. Results: Compared with the Sham group, UUO rats displayed fibrotic abnormalities, accompanied by an increased expression of α-smooth muscle actin and Fibronectin and reduced expression of E-cadherin. These molecular and pathological changes suggested increased inflammation in damaged kidneys. Oxidative stress, as evidenced by decreased levels of SOD1 and Catalase, was also observed in UUO kidneys. Additionally, activation of cleaved caspase-3 and PARP1 and increased apoptosis in the proximal tubules confirmed tubular cell apoptosis in the UUO group. All of these phenotypes exhibited by UUO rats were suppressed by treatment with BMSC-EVs. However, the protective effect of BMSC-EVs was completely abolished by the inhibition of MFG-E8. Consistent with the in vivo results, treatment with BMSC-EVs reduced inflammation, oxidative stress, apoptosis, and fibrosis in HK-2 cells stimulated with TGF-β1 in vitro. Interestingly, treatment with Y-27632 protected HK-2 cells against inflammation and fibrosis, although oxidative stress and apoptosis were unchanged. Conclusions: Our results show that BMSC-EVs containing MFG-E8 attenuate renal fibrosis in a rat model of renal fibrosis, partly through RhoA/ROCK pathway inhibition.

Background

Chronic kidney disease (CKD), and its major pathological feature renal fibrosis, is an emerging health issue worldwide[1-3]. Patients with CKD experience progressive deterioration of renal function that can progress to end-stage renal failure. Though considerable effort has been dedicated to finding ways to ameliorate renal fibrosis in these patients, few specific therapeutic strategies are available that effectively delay or prevent the progression of renal tubulointerstitial fibrosis (TIF) to end-stage renal failure[4, 5]. Bone marrow mesenchymal stem cells (BMSCs), a multipotent progenitor cell type capable of repair, regeneration, and immunomodulation, are widely seen as a promising therapeutic option for renal disease[6, 7]. For example, one trial found that activated MSCs can repair injured tissue by secreting a variety of anti-inflammatory factors. BMSCs are generally recognized for their ability to self-renew and differentiate into multiple lineages; however, this can lead to teratoma formation by transplanted BMSCs, which limits their therapeutic effectiveness[8]. Recently it has become increasingly clear that BMSC-derived extracellular vesicles (BMSC-EVs) have important biological functions and molecular

mechanisms[9], and may serve as an alternative to therapies based on BMSC transplantation[8]. EVs, which originate from BMSC endosomal compartments, can modulate inflammation[10-12]. One study showed that MSC-EVs improve renal function in several animal models of CKD. However, the biological role of BMSC-EVs–regulated renal fibrosis and the mechanism underlying this process remain elusive, and more detailed research is needed to determine the molecular functions of BMSC-EVs in this setting.

Milk fat globule-EGF factor-8 (MFG-E8), also known as lactadherin, is a secreted multifunctional glycoprotein commonly found in human milk fat globules[13, 14]. MFG-E8 has aroused widespread interest over the last decade for its role in mediating various biological processes and pathophysiological functions[15], including apoptotic clearance of dead cells in cardiovascular disease and attenuation of oxidative stress in the amelioration of early brain injury. There is growing evidence that MFG-E8 regulates the RhoA/ROCK pathway[16]. Kudo[17] et al. found that MFG-E8 inhibits the stimulatory effect of allergic inflammation on RhoA activity, thereby reducing contraction of airway smooth muscle in humans and mice[17]. MFG-E8 also regulates gastrointestinal motility by preventing RhoA activation through a PTEN-dependent mechanism[18]. In addition, Su[19] et al. found that MFG-E8, as one of the components in the secretome derived from MSCs, played anti-fibrotic function. Thus, we hypothesized that BMSCs-EVs may attenuate renal fibrosis via delivering MFG-E8, which would then regulate the RhoA/ROCK signaling pathway.

We hypothesized that BMSC-EVs may protect against inflammation, oxidative stress and apoptosis, thereby decreasing renal fibrosis. To test the hypothesis, BMSC-EVs were delivered to a rat model of unilateral ureteral obstruction (UUO). Our findings provide important insight into BMSC-EVs as a potential treatment option for CKD and clarify the mechanisms underlying their effect on renal fibrosis.

Methods

Chemicals and reagents

The primary antibodies used in our study, anti-α-SMA (ab5694), anti-Fibronectin (ab2413), anti-CD34 (ab81289), and anti-CD44 (ab189524) were obtained from Abcam (Cambridge, UK). Anti-E-cadherin (20874-1-AP), anti-SOD1 (10269-1-AP), anti-Catalase (21260-1-AP), anti-cleaved caspase-3 (19677-1-AP), and anti-PARP1(13371-1-AP) were obtained from Proteintech (Wuhan, China). Anti-RhoA (sc-418), anti-ROCK1 (sc-17794), and anti-MFG-E8 (sc-271574) were purchased from Santa Cruz Technology (California, USA). Anti-p-MYPT1 (4563T) was purchased from Cell Signaling Technology (Massachusetts, USA). Anti-CD11b (201807), anti-CD90 (206105) were purchased from Biolegend (California, USA). GAPDH (AG019) and Reactive Oxygen Species Assay Kit were obtained from Beyotime (Shanghai, China). Y-27632 (S104921) was purchased from Selleck (Texas, USA). Recombinant Human TGF-β1 (100-21) was purchased from Peprotech (New Jersey, USA). Mesenchymal Stem Cell Adipogenic Differentiation Medium (RASMX-90031), Mesenchymal Stem Cell Chondrogenic Differentiation Medium (RASMX-90041), and Mesenchymal Stem Cell Osteogenic Differentiation Medium (RASTA-90021) were

purchased from Cyagen (California, USA). RhoA Activation Assay Combo Biochem Kit (BK030) was purchased from Cytoskeleton (California, USA).

Animals

Eight-week-old male Sprague-Dawley (SD) rats (weighing 180–220 g) were used for this study. The animal experiments were approved by the Ethics Committee of Laboratory Animal Science, Shanghai Children's Medical Center, Shanghai Jiao Tong University School of Medicine (SCMCIACUC-K2019025). All rats were housed in a specific pathogen free (SPF) animal room under standard conditions with free access to water and food.

Animal experiments

Thirty male SD rats were randomly divided into six groups (n=6 in each group): the Sham group, the Sham + EVs group, the UUO group, the UUO + EVs group, the UUO + EVs^{Ctrl} group, and the UUO + $EVs^{shMFGE8}$ group. Briefly, the rats were anesthetized with 60 mg/kg pentobarbital and kept on a heated surface to maintain a body temperature of approximately 36.5°C. In the UUO group, the left ureter was exposed via abdominal incision and then ligated to the ureteral-pelvic junction with 5-0 silk sutures. In the Sham group, the left ureter was physically exposed but not ligated. The rats in the Sham and UUO groups received 0.5 mg/kg phosphate-buffered saline (PBS) vehicle intravenously. For the Sham + EVs group and the UUO + EVs group, BMSC-EVs were injected via the tail vein a day after the procedure at a dose of 0.5 mg/kg. For the UUO + EVs^{Ctrl} group, 0.5 mg/kg EVs^{Ctrl} was administered intravenously. For the UUO + $EVs^{shMFGE8}$ group, 0.5 mg/kg $EVs^{shMFGE8}$ was administered intravenously. All rats were sacrificed by pentobarbital anesthesia on postoperative day 14, and the kidneys were collected for further investigation.

BMSC isolation and culturing

BMSCs were isolated from the bone marrow of 4-week-old SD rat. The cells were cultured in DMEM supplemented with 10% fetal bovine serum and 1% penicillin-streptomycin in a 37°C incubator with 5% CO_2. The marrow was plated in T75 culture flasks, and nonadherent hematopoietic cells were removed with PBS 3 days later, followed by the addition of fresh culture medium; the medium was subsequently changed every 2–3 days. When the BMSCs reached 80%–90% confluence, they were digested with 0.25% trypsin. The cells were passaged three times prior to verification of their identity. Flow cytometry was used to screen the cells for CD44, CD90, CD11b and CD34, known markers for BMSCs. The cells were also tested for their ability to be differentiated into adipocytes, osteocytes, and chondrocytes. BMSCs at passages 3–5 were used for further experiments.

Lentiviral vector construction and transduction

To down-regulate MFG-E8 expression in BMSC-EVs, BMSCs were divided into two groups: BMSCs transfected with null lentivirus vector ($BMSCs^{Ctrl}$) and BMSCs transfected with a lentiviral vector (final

concentration, 100 nM) designed to knock down MFG-E8 expression ($BMSCs^{shMFGE8}$). Lipofectamine 2000 was used to perform the transfections. The medium was removed 24 h after transfection and replaced with fresh medium containing 10% FBS. BMSC-EVs were purified from $BMSCs^{Ctrl}$ or $BMSCs^{shMFGE8}$ as described below.

Isolation and identification of BMSC-EVs

BMSC-EVs were isolated and identified as described previously. Briefly, BMSCs at 80%–90% confluency were rinsed with PBS and cultured for 48 h in Mesen Gro MSC medium. The conditioned medium was then collected and centrifuged at 300 x g for 10 min followed by another round of centrifugation at 2000 x g for 10 min at 4 °C to remove cellular debris and dead cells. Then, the supernatant was ultra-centrifuged at 100,000 x g for 70 min at 4 °C to obtain a pellet containing the EVs, which was rinsed in 200 μl of PBS and ultracentrifuged again at 100,000 x g for another 70 min at 4 °C. The protein content of the BMSC-EVs was quantitated using a BCA Protein Assay Kit. Western blot and transmission electron microscopy (TEM) were used to examine the quality and morphology of the BMSC-EVs, and qNano was used to assess their size. The purified BMSC-EVs were stored at -80°C for later experiments.

HK-2 cell culturing and treatment

Human renal proximal tubular epithelial (HK-2) cells (XY Biotechnology, Guangzhou, China) were cultured in DMEM/F12 with 10% fetal bovine serum supplemented with 100 U/ml penicillin and 100 μg/ml streptomycin. Cells were maintained at 37 °C in a 5% CO_2/95% air atmosphere with nearly 100% relative humidity. To generate renal fibrosis cell models, the cells were incubated with TGF-β1 at a final concentration of 10 ng/ml for 72 h. After this pretreatment step, the HK-2 cells were then incubated with or without 30 μg/ml BMSC-EVs in the presence of TGF-β1. To inhibit ROCK, Y-27632 (10 μM) was added to cells treated with TGF-β1 for the final 24 h of incubation.

Renal morphology analysis

For histological examination, the kidneys were isolated, fixed in 4% formaldehyde overnight and embedded in paraffin. Hematoxylin and eosin (HE) staining was performed according to standard methods. Renal interstitial lesions were characterized by the degree of changes to the glomerulus and tubules. At least 10 randomly chosen non-overlapping fields of view at a magnification of 200 x were observed and recorded for each section. Masson's trichrome staining was used to assess the degree of renal interstitial fibrosis based on the amount of collagen deposition observed at 200 x magnification. An optical microscope equipped with image analysis software was applied to analyze images of the renal interstitium. The total area occupied by fibrotic lesions was calculated for arbitrarily chosen fields of view and expressed as the percentage of fibrotic area relative to the entire image.

Renal immunohistochemical analysis

For immunohistochemical (IHC) staining, paraffin-embedded kidney sections were rehydrated and incubated in 10 mM citrate with 0.05% Tween for antigen retrieval. After blocking, the sections were incubated with primary antibody at 4°C overnight, followed by incubation with a horseradish peroxidase–conjugated secondary antibody for 1 h at 37°C. All images were recorded using Image-Pro Plus 6.0.

RhoA activation assay

The RhoA activation assay was performed using a GTP pulldown assay kit according to the manufacturer's instructions. After cells were lysed, 300–500 μg of total protein was added to 10 μL RBD-binding beads, then incubated at 4°C on a rotator for 1 h, washed three times with PBS, and resuspended in Laemmli buffer. Finally, the protein samples were heated at 100 °C for 10 min and stored at -20 °C.

Western blot

Total protein was extracted by suspending kidney tissues in ice-cold RIPA buffer containing a protease inhibitor cocktail, followed by homogenization and subsequent centrifuged at 12000 x g for 20 min, after which the pellets were discarded and the protein concentration was quantified using t a bicinchoninic acid (BCA) assay method. Next, a 4 x volume of loading buffer was added each to supernatant for Western blot. Equal amounts of each protein sample (40 μg/lane) were loaded onto a 8%–12% SOD1ium dodecyl sulfate-polyacrylamide gel, electrophoresed for 2 h and then transferred to poly-vinylidene fluoride membrane. The membranes were blocked for 1.5 h at room temperature with 5% nonfat milk followed by incubation at 4 °C overnight with primary antibodies against the following proteins: α-SMA, E-cadherin, Fibronectin, Catalase, SOD1, cleaved caspase-3, PARP1, and GAPDH. The membranes were then incubated with an HRP-conjugated goat anti-mouse secondary antibody or with rabbit lgG. The protein bands were detected by enhanced chemiluminescence (ECL) and imaged. Semi-quantitative analysis was performed by measuring band intensities for three experiments using ImageJ software.

Quantitative real-time PCR

Total RNA was isolated from kidney tissues using TRIzol according to the standard protocol. Reverse transcription was carried out to synthesize complementary DNA (cDNA) from 500 ng total RNA using 5 x primescript RT Master Mix 2 μl (TAKARA) in a 10-μl reaction volume. The quantitative real-time PCR reaction was performed using qPCR Master Mix, (TAKARA, Japan), primers (designed and synthesized by Shanghai Sangon Biological Co, Ltd), and RNase-Free ddH_2O in a 10-μl reaction volume. An Applied Biosystems® 7500 Fast Real-time PCR System was used to run the following program: 95 °C for 30 seconds, 40 cycles of 95 °C for 5 seconds and 60 °C for 34 seconds, followed by 95 °C for 15 seconds, 60°C for 1 min and 95 °C for 15 seconds. The threshold cycle (Ct) was recorded by the instrument's software (7500), and fold changes in mRNA expression were calculated according to the comparative Ct method ($2^{-}\triangle\triangle CT$). Results were normalized to mRNA expression in the kidney tissues of rats from the Sham group. The rat primers used for RT-PCR were as follows: α-SMA, forward 5'-CAGGGAGTGATGGTTGGAAT -3' and reverse 5'-GGTGATGATGCCGTGTTCTA-3';E-cadherin, forward 5'-CTCAGTGTTTGCTCGGCGTTTGC-3' and reverse 5'-GCTCTGGGTTGGATTCAGAG-3'; Fibronectin, forward

5’-GATTCTTCTGGCGTCTGCAC-3’ and reverse 5’-GCCCCGGAACATGAGGATAG-3’; IL-1β, forward 5’-AGCAGCTTTCGACAGTGAGG-3’ and reverse 5’-CTCCACGGGCAAGACATAGG-3’; IL-6, forward 5’—3’ and reverse 5’—3’; TNF-α, forward 5’-CAACCAGGCCATCAGCAACAACAT-3’ and reverse 5’-TCTGTGGGTTGTTCACCTCGAACT-3’; IL-10, forward 5’-GGACTTTAAGGGTTACTTGGG-3’ and reverse 5’-AGAAATCGATGACAGCGTCG-3’; GAPDH, forward 5’-TGACTCTACCCACGGCAAGTTCAA-3’ and reverse 5’-ACGACATACTCAGCACCAGCATCA-3’.

Measurement of oxidative stress

Oxidative stress in kidney tissues was determined by Western blot analysis of SOD1 and Catalase expression. Oxidative stress in HK-2 cells was assessed using the oxidation-sensitive probe DCFH-DA, as previously described. After culturing under various conditions, the ROS levels in HK-2 cells from each group were assessed using the ROS detection kit. The cells were cultured with DCFH-DA for 20 min at 37 °C. After washing with PBS three times, the ROS levels were observed using a fluorescent microscope.

Analysis of apoptosis

Apoptosis in kidney tissues and HK-2 cells was assessed using different three methods. First, apoptosis in kidney tissues was determined by Western blot analysis of cleaved caspase-3 and PARP expression. Second, a TUNEL assay was performed using an *in situ* Cell Death Detection kit according to the manufacturer’s instruction (Roche Applied Science, Indianapolis, IN) to examine apoptosis in kidney tissues. The number of apoptotic cells was counted under a fluorescent microscope at 200 x magnification. At least 10 areas around the proximal tubules from sections from different rats from each group were counted and averaged. Third, HK-2 cell apoptosis was detected by flow cytometry using an Annexin V-FITC/PI Apoptosis Detection Kit. The cells were collected and re-suspended at 1 x 10^6 in 300 μl of binding buffer. Then, 10 μl PI solution and 5 μl Annexin V-FITC solution were added, and the cells were incubated for 5 min. A total of 10,000 events were collected, and the proportion of apoptotic cells was analyzed by flow cytometry.

Statistical analysis

Data are presented as the mean ± standard deviation (SD). Significant differences were examined by one-way analysis of variance with Bonferroni correction; p 0.05 was deemed to be statistically significant. All statistical analyses were performed using SPSS version 20.0 statistical software.

Results

Characterization of BMSCs and BMSC-EVs

Third- to fifth-generation BMSCs were used in our study. The cells were long and spindle-shaped (Fig. 1B), which is highly consistent with previous reports. Flow cytometry analysis showed that these cells exhibited high levels of the characteristic markers CD90 and CD44 (99.79% and 55.71% respectively), and

very low levels of CD34 and CD11b (0.08% and 0.01% respectively) (Fig. 1A). Third-generation cells were successfully differentiated into adipogenic, osteogenic and chondrogenic cells (Fig. 1C). These results indicate that the BMSCs were successfully isolated and cultured. The isolated BMSC-EVs exhibited typical cup-shaped morphology with a diameter of approximately 40–150 nm when observed by transmission electron microscopy (Fig. 1E, F), and expressed high levels of the characteristic marker proteins CD9, CD63 and HSP70, as detected by Western blot (Fig. 1D).

Treatment with BMSC-EVs reduces pathological changes and renal fibrosis in UUO rats

To investigate whether intravenous administration of BMSC-EVs protects against renal fibrosis in UUO rats, we first assessed pathological changes and collagen deposition by HE and Masson's trichrome staining. As shown in Fig. 2A, we found infiltration of inflammatory cells and severe structural damage, such as tubular dilation, tubular atrophy and glomerular enlargement in the kidneys from UUO rats. Consistent with the HE staining results, Masson's trichrome staining revealed severe interstitial collagen deposition in the obstructed kidneys (Fig. 2B). In the group treated with BMSC-EVs, we observed fewer dilated tubules, less substantially atrophied parenchyma and reduced collagen deposition compared with untreated rats (Fig. 2B). Next, we analyzed the expression of fibrotic biomarkers including α-SMA, E-cadherin and Fibronectin. The protein and mRNA levels of α-SMA and Fibronectin were clearly increased, while E-cadherin expression was markedly decreased at both the mRNA and protein level in the UUO kidneys (Fig. 3A, B). In addition, strikingly high levels of α-SMA and Fibronectin expression and considerably less E-cadherin expression were detected in the kidneys of UUO rats compared with control rats, as determined by IHC staining (Fig. 2E). However, intravenous administration of BMSC-EVs could prevent these changes in fibrotic factor expression in UUO kidneys (Fig. 2E, 3A, B). Overall, these results indicated that treatment with BMSC-EVs can protect against UUO-induced renal pathological changes and fibrosis.

Treatment with BMSC-EVs protects UUO kidneys against inflammation, oxidative stress and apoptosis

Progressive inflammation promotes collagen deposition, resulting in TIF in UUO kidneys. Thus, we investigated the effect of BMSC-EVs treatment on inflammation in UUO kidneys. The RT-PCR results showed that the inflammatory cytokines IL-1β, TNF-α, IL-6, and IL-10 were significantly overexpressed in kidneys from UUO rats compared with kidney from normal control rats. As is shown in Fig. 2D, mRNA levels of the former three of these factors were reduced by treatment with BMSC-EVs, while the expression of IL-10 mRNA was not altered. Moreover, treatment with BMSC-EVs effectively reduced the elevated expression of the macrophage marker ED-1 in the UUO kidneys (Fig. 2C). These results show that treatment with BMSC-EVs reduced inflammation and macrophage infiltration in UUO kidneys. Oxidative stress is associated with renal fibrosis progression in UUO rats. Therefore, we next investigated the effect of BMSC-EVs treatment on oxidative stress–related molecules in the UUO kidneys. As shown in Fig. 3C, the protein expression levels of the antioxidant enzymes SOD1 and Catalase were significantly reduced in UUO kidneys, whereas treatment with BMSC-EVs results in the up-regulation of these two proteins. These results suggest that treatment with BMSC-EVs diminished oxidative stress in UUO

kidneys. There is increasing evidence that apoptosis, which can trigger further inflammatory reactions, plays a pathogenic role in UUO-induced renal fibrosis. To explore the role of BMSC-EVs in renal cell apoptosis, the expression of renal apoptosis–related proteins were assessed by Western blot. Compared with the Sham group, the protein levels of cleaved caspase-3 and PARP1 were clearly up-regulated in the UUO group, and treatment with BMSC-EVs significantly suppressed the expression of these two proteins, as shown in Fig. 3C. Furthermore, the number of TUNEL-positive cells in the proximal tubules of the kidneys was clearly elevated in the UUO group compared with the Sham group, and this effect was dramatically reduced by administration of BMSC-EVs (Fig. 3D). Overall these results suggest that BMSC-EVs suppress inflammation, oxidative stress, and apoptosis.

BMSC-EVs inhibit TGF-β1-induced activation of HK-2 cells

Next, we treated HK-2 cells with TGF-β1 (10 ng/ml) for 72 h to induce fibrosis and investigated the protective effect of BMSC-EVs against fibrosis, inflammation, oxidative stress and apoptosis in vitro. To examine the effect of BMSC-EVs on the epithelial mesenchymal transition (EMT), epithelial markers and mesenchymal markers were assessed by Western blot. We found that treatment with BMSC-EVs triggered a clear decrease in the expression of the mesenchymal markers α-SMA and Fibronectin, while expression of the epithelial marker E-cadherin was increased compared with HK-2 cells stimulated by TGF-β1 but not treated with BMSC-EVs (Fig. 4A). Moreover, TGF-β1 induced a clear increase in proinflammatory molecule secretion, as observed in the in vivo experiment described above. However, the increased secretion of these proinflammatory molecules was suppressed by treatment with BMSC-EVs (Fig. 4B). As for oxidative stress, treatment with BMSC-EVs declined TGF-β1-induced ROS production in HK-2 cells, as shown in Fig. 4C. Consistent with the reduction in oxidative stress, cell apoptosis was significantly reduced in cells treated with BMSC-EVs, as assessed by flow cytometry with Annexin V-FITC/PI double staining, which was similar to the results from the in vivo experiment (Fig. 4D).

Identification of candidate anti-fibrotic factors activated by treatment with BMSC-EVs

MFG-E8 has been implicated in the MSC-EV–mediated amelioration of liver fibrosis[19]; however, it is unknown whether it plays a role in renal fibrosis. To determine whether MFG-E8 is involved in the effects observed in response to treatment with BMSC-EVs, we first assessed MFG-E8 expression in BMSC-EVs by Western blot. As expected, MFG-E8 was expressed at high levels in BMSC-EVs (Fig. 5A). Next, BMSCs were transfected with lentiviral vectors expressing MFG-E8 shRNAs to silence MFG-E8 expression, and Western blot showed that MFG-E8 expression in MFGE8-silenced BMSC-EVs was effectively silenced (Fig. 5A).

We next examined the effect of MFGE8–silenced BMSC-EVs in renal TIF induced by UUO. HE staining revealed more severe renal damage in kidneys from rats treated with MFGE8–silenced BMSC-EVs compared with those from rats treated with normal BMSC-EVs (Fig. 5B). Masson's trichrome staining showed increased extracellular matrix deposition after treatment with MFGE8–silenced BMSC-EVs compared with normal BMSC-EVs (Fig. 5C). As shown in Fig. 6A, B, D, α-SMA and Fibronectin protein and mRNA levels were markedly increased in the UUO group treated with MFGE8–silenced BMSC-EVs

compared with the UUO group treated with normal BMSC-EVs, whereas E-cadherin protein and mRNA levels were markedly decreased. Immunohistochemical staining revealed similar results (Fig. 5F). In addition, RT-PCR analysis showed that the levels of proinflammation-related factors were significantly higher in the group treated with MFGE8–silenced BMSC-EVs compared with normal BMSC-EVs (Fig. 5E), and treatment with MFGE8–silenced BMSC-EVs did not altered the elevated expression of the macrophage marker ED-1 in the UUO kidneys (Fig. 5D). Next, we evaluated the expression of oxidative stress–related proteins. The expression levels of SOD1 and Catalase were lower in the group treated with MFGE8–silenced BMSC-EVs compared with normal BMSC-EVs (Fig. 6C, E). Furthermore, a greater degree of apoptosis was seen in the group treated with MFGE8–silenced BMSC-EVs compared with normal BMSC-EVs, as shown in Fig. 6C, F. Taken together, these results suggest that MFGE8–silenced BMSC-EVs provided little protection to the adverse renal effects induced by UUO.

MFG-E8 expressed by BMSC-EVs attenuates fibrosis in HK-2 cells by inhibiting RhoA/ROCK signaling

We next explored the molecular mechanism underlying the beneficial effects of treatment with BMSC-EVs on renal fibrosis. To determine whether RhoA/ROCK signaling is involved in TGF-β1–induced activation of HK-2 cells, we performed a RhoA activity assay for RhoA activation and used Western blot to test MYPT1. MYPT1 is the major effector of ROCK1, so we assessed the MYPT1 phosphorylation as an indicator of ROCK1 activity. The level of activated GTP-bound RhoA was dramatically increased after co-culturing with TGF-β1, whereas treatment with BMSC-EVs attenuated TGF-β1–mediated RhoA activation (Fig. 7B). In addition, there was an approximately 3.5-fold increase in p-MYPT1 levels in the TGF-β1 group compared with the unstimulated HK-2 cells. Consistent with this, treatment with BMSC-EVs attenuated the increase in p-MYPT1 levels in the TGF-β1 + BMSC-EVs group (Fig. 7B).

To further verify the role of RhoA/ROCK pathway in regulating TGF-β1–induced activation of HK-2 cells, we treated cells with the ROCK inhibitor Y-27632. Compared with the UUO group, the UUO group treated with Y-27632 exhibited higher E-cadherin expression levels and lower α-SMA and Fibronectin expression levels, similar to the effect of BMSC-EVs (Fig. 7A, D). Furthermore, administration of Y-27632 significantly reversed the changes in inflammatory cytokine expression levels (Fig. 7C). In addition, Western blot analysis revealed the upregulation of GTP-bound RhoA and its downstream molecule p-MYPT1 in HK-2 cells stimulated by TGF-β1 (Fig. 7B, E). However, there was no change in TGF-β1–induced oxidative-stress or renal cell apoptosis (Fig. 7F, G). These results indicate that treatment with Y-27632 can decrease fibrosis and inflammation but not oxidative stress or cell apoptosis in TGF-β1–induced HK-2 cells.

Discussion

In this study, we found that BMSC-EVs can reduce renal fibrosis by producing MFG-E8, which inhibits the RhoA/ROCK pathway.

Renal fibrosis, which is characterized by unchecked deposition of fibrotic matrix in the interstitial compartment, is a characteristic feature of CKD[20, 21]. Renal fibrosis develops in response to a host of insults such as growth factors and stress molecules, and the development goes through several

important phases, including activation of renal interstitial fibroblasts, excessive and progressive accumulation of extracellular matrix (ECM)[22], EMT[23], inflammatory cell infiltration and tubular cell apoptosis[24]. During the chronic injury that occurs in CKD, continuous fibrotic matrix deposition will disrupt organ structure, suppress blood supply, affect organ function, and ultimately cause kidney failure[25, 26].

Because of the severe consequences of renal fibrosis, an increasing number of studies have focused on developing effective treatments for this condition[27]. For example, numerous studies have tested the usefulness of treatment with TGF-β inhibitors, as TGF-β signaling is an important mediator of renal fibrosis, although the clinical applications of this approach are limited because of the role of TGF-β in cancer[28, 29]. Apart from TGF-β inhibitors, an anti-CTCF monoclonal antibody, the small molecule AA123 that mimics BMP-7, and Gal-3 inhibitors all performed poorly in clinical trials[30]. Unilateral ureteral obstruction (UUO) and TGF-β1-induction of HK-2 cells are well-established *in vivo* and *in vitro* models[31-33], respectively, of human renal fibrosis that have been used extensively by researchers to better understand the pathogenesis of this devastating disease. In this study, a UUO-induced rat model of tubulointerstitial fibrosis and TGF-β1–induced HK-2 cells were used to test the therapeutic effect of BMSC-EVs and its underlying mechanisms.

Numerous studies have reported that BMSCs can induce tissue regeneration after injury[7, 34]. Recently, much attention has been paid to stem cell therapy in fibrosis[7]. Zhang[35] et al. showed that BMSCs aggravate silica-induced pulmonary fibrosis, potentially by attenuating Wnt/β-catenin signaling, in rats. Liu and Zheng[34] found that BMSC transplantation attenuates inflammation, oxidative stress, and fibrosis in skeletal muscle after muscle contusion. In addition, BMSC infusion has been reported to improve recovery from the acute kidney injury (AKI) induced by ischemia/reperfusion[10]. However, BMSCs can also be tumorigenic and are often inappropriately retained by target tissues, limiting their clinical usefulness[9]. Emerging data suggest that BMSCs may promote regeneration in a paracrine/endocrine manner by delivering EVs to specific tissues[8].

EVs, which are typically approximately 40–200 nm in size[10], can be categorized as exosomes, microvesicles and apoptotic bodies. EVs are membranous bodies that are released by almost all cells[8]. For a long time, EVs were considered to be debris without any biological function. Recently, however, EVs have attracted great attention in the field of organ regeneration because of the information they package that enables cell-cell communication via fusion with the recipient cell membrane and transfer of biomolecules, such as nucleic acids and proteins[10]. Intra-renal MSC-EVs delivery attenuates tissue inflammation and microvascular loss, which in turn improves stenotic-kidney hemodynamics. EVs release and uptake have important physiological functions, and can contribute to the development of inflammatory, malignant and infectious diseases[36, 37]. EVs are increasingly recognized for their role in regulating numerous biological processes, which they carry out by transferring a variety of immune modulators such as proteins, mRNAs, microRNAs and lipids, thus shuttling selected information to recipient cells[38, 39]. This process may represent an alternative approach to stem cell therapy that could help attenuate disease progression.

It is widely accepted that inflammation plays a vital role in the initiation and progression of renal injury in chronic renal fibrosis[40, 41], which eventually leads to the destruction of renal parenchyma. Previous studies have shown that damaged tubular epithelial cells recruit inflammatory cells to the renal interstitial compartment, resulting in the production of a myriad of proinflammatory and pro-fibrotic cytokines by the infiltrated inflammatory cells, which then act on renal tubular epithelial cells to promote renal fibrosis. Chemokines like tumor necrosis factor-α (TNF-α) mediate inflammatory cell infiltration and fibroblast recruitment[42, 43], which can be inhibited by BMSCs, thus preventing subsequent inflammatory responses. In our study, we found that the expression of inflammatory cytokines like TNF-α, IL-6, IL-10 and IL-1β was increased in UUO kidneys and reversed by treatment with BMSC-EVs. However, the expression of cytokine IL-10, was not clearly decreased by treatment with BMSC-EVs, which may reflect the differential effect of BMSC-EVs in preventing inflammation. We also examined macrophage infiltration in the obstructed kidney by ED-1 staining, which detects active monocytes/macrophages, and found that treatment with BMSC-EVs clearly and effectively protects against UUO-induced renal fibrosis by inhibiting the inflammatory response.

In addition to the inflammatory response, elevated oxidative stress is another pivotal cause of renal fibrosis[37]. Oxidative stress is an imbalance between the oxidation system and the endogenous antioxidant defense system that results in ATP depletion. As described in previous reports, UUO is linked to reduced levels of the antioxidative enzymes SOD1 and Catalase[44, 45]. Our findings confirmed these results, as detected by Western blot of *in vivo* samples and DCFH-DA probe analysis of *in vitro* samples. Our *in vivo* data showed that UUO operation largely suppressed the activities of the antioxidant enzymes SOD1 and Catalase. Intravenous injection of BMSC-EVs helped restore the activity of these enzymes. The *in vitro* results were consistent with these findings. Therefore, our findings show that oxidative stress was significantly reduced after BMSC-EVs treatment both *in vivo* and *in vitro*.

Oxidative stress can also induce cell apoptosis. Apoptosis, a key pathological process in renal fibrosis, can be triggered either by either extrinsic or intrinsic pathways[3, 46, 47]. If apoptotic cells are not quickly cleared, secondary necrosis will occur, which can lead to further damage[48]. Therefore, inhibition of cell apoptosis may be an effective treatment for renal fibrosis. We detected high levels of activated caspase-3 and PARP1 in obstructed kidneys that were reversed by treatment with BMSC-EVs. Moreover, treatment with BMSC-EVs decreased the cell population labeled by Annexin-V, indicating a reduction in apoptosis. Previous studies have shown that SOD1 and Catalase reduce the expression of pro-apoptotic molecules such as activated caspase-3 and PARP1, suggesting that BMSC-EVs suppress oxidation-induced apoptosis by inhibiting the intrinsic apoptotic pathway.

Though numerous kinds of EVs may play an influential role in fibrosis, there are still variations in therapeutic outcomes, which could be partly explained by differences in the levels of beneficial and harmful factors contained in the EVs[19]. Therefore, identifying the beneficial compounds contained in EVs is critical for developing more efficient therapies. Among the numerous proteins associated with EVs, MFG-E8 has generated great interest based on its potential ability to attenuate fibrosis[19]. MFG-E8, a soluble glycoprotein, is a vital factor in diverse physiological processes, including reducing inflammation,

clearance of apoptotic cells, and angiogenesis[49, 50]. Several recent studies have confirmed the therapeutic potential of MFG-E8 in various renal diseases, such as renal ischemia-reperfusion injury and sepsis-induced acute kidney disease[51]. MFG-E8 has also been shown to protect the kidneys by suppressing inflammation and apoptosis[52, 53]. Moreover, MFG-E8 plays an essential role in macrophage reprogramming through the induction of the anti-inflammatory M2 phenotype[19]. However, it is unclear whether MFG-E8 is one of the key molecules in the EVs that contributes to fibrotic regression. Western blot analysis confirmed that BMSC-EVs secreted high levels of MFG-E8. We therefore hypothesized that MFG-E8 was the most likely effector of BMSC-EVs–mediated nephroprotection.

The results from our *in vivo* investigation of the potential nephroprotective effect of MFG-E8 were quite unexpected. Because MFG-E8 was just one of many compounds contained in EVs, we expected MFGE8–silenced BMSC-EVs to exhibit only a partial reduction in nephroprotection. Unexpectedly, however, the nephroprotective effects of the EVs virtually disappeared following transfection with the lentivirus. Our *in vivo* results demonstrated that MFGE8–silenced BMSC-EVs have a very low ability to protect obstructed kidneys compared with BMSC-EVs. Therefore, our findings show that MFG-E8 is a key extracellular vesicle molecule that contributes to fibrotic regression.

Our findings also suggest a mechanistic basis for how BMSC-EVs exert their nephroprotective effects. Many studies have illustrated the importance of RhoA/ROCK signaling in regulating fibrosis, so we hypothesized that the RhoA/ROCK pathway may contribute to BMSC-EVs–mediated nephroprotection. Consistent with expectation, we found that BMSC-EVs downregulated RhoA/ROCK expression *in vitro*. Interestingly, while treatment with Y-27632, a ROCK1 inhibitor, reversed TGF-β1–induced inflammation and fibrosis in HK-2 cells, it had little effect on oxidative stress and apoptosis. Thus, further research is needed to identify the pathway involved in BMSC-EV–mediated downregulation of oxidative stress and apoptosis in renal fibrosis.

There were two limitations to our study. First, we did not assess renal function. However, many previous studies have reported that BUN and serum creatinine are not significantly affected by UUO because of the presence of the intact contralateral kidney, indicating that BUN and serum creatinine are not good indicators of renal function in an animal model of UUO[4, 27]. Second, while our study showed that BMSC-EVs reduce renal fibrosis in part by inhibiting RhoA/ROCK, further research is needed to determine how BMSC-EVs exert antioxidant and antiapoptotic activities in the context of renal fibrosis.

Conclusions

In summary, our findings show that EVs derived from BMSCs can attenuate renal fibrosis. More significantly, we present a novel mechanism by which BMSC-EVs deliver MFG-E8 to renal cells and inhibit inflammation, oxidative stress, apoptosis and fibrosis, in part by downregulating the RhoA/ROCK pathway. This study highlights the potential therapeutic usefulness of BMSC-EVs in clinical applications.

Abbreviations

CKD: Chronic kidney disease; BMSCs: Bone marrow mesenchymal stem cells; EVs: Extracellular vesicles; MFG-E8: milk fat globule-EGF factor-8; UUO: unilateral ureteral obstruction; SD: Sprague-Dawley; TGF-β1: Transforming growth factor-β1; TIF: Tubulointerstitial fibrosis; SPF: Specific pathogen free; PBS: Phosphate-buffered saline; TEM: Transmission electron microscopy; HK-2: Human renal proximal tubular epithelial; HE: Hematoxylin and eosin; IHC: Immunohistochemical; BCA: Bicinchoninic acid; ECL: Enhanced chemiluminescence; EMT: Epithelial mesenchymal transition; ECM: Extracellular matrix; TNF-α: Tumor necrosis factor-α

Declarations

Ethics approval and consent to participate

The animal experiments were approved by the Ethics Committee of Laboratory Animal Science, Shanghai Children's Medical Center, Shanghai Jiao Tong University School of Medicine (SCMCIACUC-K2019025).

Consent for publication

Not applicable.

Availability of data and materials

All data generated or analyzed during this study are included in this published article.

Competing interests

The authors declare that they have no competing interests.

Funding

This work was supported by grants from the National Nature Science Foundation of China (grant number: 81972139), Natural Science Foundation of Shanghai (grant number: 19ZR1432800), and the Program for improving the Clinical Scientific Research ability of Postgraduate students in Pediatrics, Shanghai Jiao Tong University School of Medicine (grant number: EKKY2018005DGD).

Authors' contributions

ZZS designed the study, conducted the experiments, analyzed the data, interpreted the data, wrote the manuscript, and provided approval for the final version of the manuscript. QW interpreted the data and provided approval for the final version of the manuscript. YBZ interpreted the data, wrote the manuscript, and provided approval for the final version of the manuscript. DPJ designed the study, conducted experiments, wrote the manuscript, and provided approval for the final version of the manuscript.

Acknowledgements

We thank Dr. Emily Crow for his suggestions to revise the manuscript.

Authors details

[1]Department of Urology, Shanghai Children's Medical Center, Shanghai Jiao Tong University School of Medicine, Shanghai, China

[2]Department of Pediatric Surgery, Nantong Maternal and Child Health Hospital, Nantong, Jiangsu, China

References

1. Mazzei L, Docherty NG, Manucha W. Mediators and mechanisms of heat shock protein 70 based cytoprotection in obstructive nephropathy. Cell stress & chaperones. 2015;20(6):893-906.
2. Tse G, Yan BP, Chan YW, Tian XY, Huang Y. Reactive Oxygen Species, Endoplasmic Reticulum Stress and Mitochondrial Dysfunction: The Link with Cardiac Arrhythmogenesis. Frontiers in physiology. 2016;7:313.
3. Zhao H, Liu YJ, Liu ZR, Tang DD, Chen XW, Chen YH, et al. Role of mitochondrial dysfunction in renal fibrosis promoted by hypochlorite-modified albumin in a remnant kidney model and protective effects of antioxidant peptide SS-31. European journal of pharmacology. 2017;804:57-67.
4. Lee HJ, Gonzalez O, Dick EJ, Donati A, Feliers D, Choudhury GG, et al. Marmoset as a Model to Study Kidney Changes Associated With Aging. The journals of gerontology Series A, Biological sciences and medical sciences. 2019;74(3):315-24.
5. Kim SM, Kim YG, Kim DJ, Park SH, Jeong KH, Lee YH, et al. Inflammasome-Independent Role of NLRP3 Mediates Mitochondrial Regulation in Renal Injury. Frontiers in immunology. 2018;9:2563.
6. Teo AQA, Wong KL, Shen L, Lim JY, Toh WS, Lee EH, et al. Equivalent 10-Year Outcomes After Implantation of Autologous Bone Marrow-Derived Mesenchymal Stem Cells Versus Autologous Chondrocyte Implantation for Chondral Defects of the Knee. The American journal of sports medicine. 2019;47(12):2881-7.

7. Li X, Wu A, Han C, Chen C, Zhou T, Zhang K, et al. Bone marrow-derived mesenchymal stem cells in three-dimensional co-culture attenuate degeneration of nucleus pulposus cells. Aging. 2019;11(20):9167-87.
8. Li J, Ding Z, Li Y, Wang W, Wang J, Yu H, et al. BMSCs-Derived Exosomes Ameliorate Pain Via Abrogation of Aberrant Nerve Invasion in Subchondral Bone in Lumbar Facet Joint Osteoarthritis. Journal of orthopaedic research : official publication of the Orthopaedic Research Society. 2019.
9. Qin F, Tang H, Zhang Y, Zhang Z, Huang P, Zhu J. Bone marrow-derived mesenchymal stem cell-derived exosomal microRNA-208a promotes osteosarcoma cell proliferation, migration, and invasion. Journal of cellular physiology. 2019.
10. Zhu G, Pei L, Lin F, Yin H, Li X, He W, et al. Exosomes from human-bone-marrow-derived mesenchymal stem cells protect against renal ischemia/reperfusion injury via transferring miR-199a-3p. Journal of cellular physiology. 2019;234(12):23736-49.
11. Go V, Bowley BGE, Pessina MA, Zhang ZG, Chopp M, Finklestein SP, et al. Extracellular vesicles from mesenchymal stem cells reduce microglial-mediated neuroinflammation after cortical injury in aged Rhesus monkeys. GeroScience. 2019.
12. Grange C, Skovronova R, Marabese F, Bussolati B. Stem Cell-Derived Extracellular Vesicles and Kidney Regeneration. Cells. 2019;8(10).
13. Kanemura T, Miyata H, Makino T, Tanaka K, Sugimura K, Hamada-Uematsu M, et al. Immunoregulatory influence of abundant MFG-E8 expression by esophageal cancer treated with chemotherapy. Cancer science. 2018;109(11):3393-402.
14. Weise SC, Villarreal A, Heidrich S, Dehghanian F, Schachtrup C, Nestel S, et al. TGFbeta-Signaling and FOXG1-Expression Are a Hallmark of Astrocyte Lineage Diversity in the Murine Ventral and Dorsal Forebrain. Frontiers in cellular neuroscience. 2018;12:448.
15. Li H, Guan K, Li X, Ma Y, Zhou S. MFG-E8 induced differences in proteomic profiles in mouse C2C12 cells and its effect on PI3K/Akt and ERK signal pathways. International journal of biological macromolecules. 2019;124:681-8.
16. Moon HG, Cao Y, Yang J, Lee JH, Choi HS, Jin Y. Lung epithelial cell-derived extracellular vesicles activate macrophage-mediated inflammatory responses via ROCK1 pathway. Cell death & disease. 2015;6:e2016.
17. Kudo M, Khalifeh Soltani SM, Sakuma SA, McKleroy W, Lee TH, Woodruff PG, et al. Mfge8 suppresses airway hyperresponsiveness in asthma by regulating smooth muscle contraction. Proceedings of the National Academy of Sciences of the United States of America. 2013;110(2):660-5.
18. Khalifeh-Soltani A, Ha A, Podolsky MJ, McCarthy DA, McKleroy W, Azary S, et al. alpha8beta1 integrin regulates nutrient absorption through an Mfge8-PTEN dependent mechanism. eLife. 2016;5.
19. An SY, Jang YJ, Lim HJ, Han J, Lee J, Lee G, et al. Milk Fat Globule-EGF Factor 8, Secreted by Mesenchymal Stem Cells, Protects Against Liver Fibrosis in Mice. Gastroenterology. 2017;152(5):1174-86.

20. Zhou B, Mu J, Gong Y, Lu C, Zhao Y, He T, et al. Brd4 inhibition attenuates unilateral ureteral obstruction-induced fibrosis by blocking TGF-beta-mediated Nox4 expression. Redox biology. 2017;11:390-402.
21. Meng J, Li L, Zhao Y, Zhou Z, Zhang M, Li D, et al. MicroRNA-196a/b Mitigate Renal Fibrosis by Targeting TGF-beta Receptor 2. Journal of the American Society of Nephrology : JASN. 2016;27(10):3006-21.
22. Furini G, Schroeder N, Huang L, Boocock D, Scarpellini A, Coveney C, et al. Proteomic Profiling Reveals the Transglutaminase-2 Externalization Pathway in Kidneys after Unilateral Ureteric Obstruction. Journal of the American Society of Nephrology : JASN. 2018;29(3):880-905.
23. Livingston MJ, Ding HF, Huang S, Hill JA, Yin XM, Dong Z. Persistent activation of autophagy in kidney tubular cells promotes renal interstitial fibrosis during unilateral ureteral obstruction. Autophagy. 2016;12(6):976-98.
24. Wang B, Yao K, Huuskes BM, Shen HH, Zhuang J, Godson C, et al. Mesenchymal Stem Cells Deliver Exogenous MicroRNA-let7c via Exosomes to Attenuate Renal Fibrosis. Molecular therapy : the journal of the American Society of Gene Therapy. 2016;24(7):1290-301.
25. Wang P, Luo ML, Song E, Zhou Z, Ma T, Wang J, et al. Long noncoding RNA lnc-TSI inhibits renal fibrogenesis by negatively regulating the TGF-beta/Smad3 pathway. Science translational medicine. 2018;10(462).
26. Xiong C, Guan Y, Zhou X, Liu L, Zhuang MA, Zhang W, et al. Selective inhibition of class IIa histone deacetylases alleviates renal fibrosis. FASEB journal : official publication of the Federation of American Societies for Experimental Biology. 2019;33(7):8249-62.
27. Liu F, Zhuang S. New Therapies for the Treatment of Renal Fibrosis. Advances in experimental medicine and biology. 2019;1165:625-59.
28. Klinkhammer BM, Goldschmeding R, Floege J, Boor P. Treatment of Renal Fibrosis-Turning Challenges into Opportunities. Advances in chronic kidney disease. 2017;24(2):117-29.
29. Meng XM, Tang PM, Li J, Lan HY. TGF-beta/Smad signaling in renal fibrosis. Frontiers in physiology. 2015;6:82.
30. Sugimoto H, LeBleu VS, Bosukonda D, Keck P, Taduri G, Bechtel W, et al. Activin-like kinase 3 is important for kidney regeneration and reversal of fibrosis. Nature medicine. 2012;18(3):396-404.
31. Cao W, Yuan Y, Liu X, Li Q, An X, Huang Z, et al. Adenosine kinase inhibition protects against cisplatin-induced nephrotoxicity. American journal of physiology Renal physiology. 2019;317(1):F107-f15.
32. Feng X, Zhao J, Ding J, Shen X, Zhou J, Xu Z. LncRNA Blnc1 expression and its effect on renal fibrosis in diabetic nephropathy. American journal of translational research. 2019;11(9):5664-72.
33. Martinez-Klimova E, Aparicio-Trejo OE, Tapia E, Pedraza-Chaverri J. Unilateral Ureteral Obstruction as a Model to Investigate Fibrosis-Attenuating Treatments. Biomolecules. 2019;9(4).
34. Liu X, Zheng L, Zhou Y, Chen Y, Chen P, Xiao W. BMSC Transplantation Aggravates Inflammation, Oxidative Stress, and Fibrosis and Impairs Skeletal Muscle Regeneration. Frontiers in physiology.

2019;10:87.

35. Zhang E, Yang Y, Chen S, Peng C, Lavin MF, Yeo AJ, et al. Bone marrow mesenchymal stromal cells attenuate silica-induced pulmonary fibrosis potentially by attenuating Wnt/β-catenin signaling in rats. Stem cell research & therapy. 2018;9(1):311-.
36. Ma J, Zhao Y, Sun L, Sun X, Zhao X, Sun X, et al. Exosomes Derived from Akt-Modified Human Umbilical Cord Mesenchymal Stem Cells Improve Cardiac Regeneration and Promote Angiogenesis via Activating Platelet-Derived Growth Factor D. Stem cells translational medicine. 2017;6(1):51-9.
37. Zhou Y, Xu H, Xu W, Wang B, Wu H, Tao Y, et al. Exosomes released by human umbilical cord mesenchymal stem cells protect against cisplatin-induced renal oxidative stress and apoptosis in vivo and in vitro. Stem cell research & therapy. 2013;4(2):34.
38. Shojaei S, Hashemi SM, Ghanbarian H, Salehi M, Mohammadi-Yeganeh S. Effect of mesenchymal stem cells-derived exosomes on tumor microenvironment: Tumor progression versus tumor suppression. Journal of cellular physiology. 2019;234(4):3394-409.
39. Wang B, Jia H, Zhang B, Wang J, Ji C, Zhu X, et al. Pre-incubation with hucMSC-exosomes prevents cisplatin-induced nephrotoxicity by activating autophagy. Stem cell research & therapy. 2017;8(1):75.
40. Li YZ, Ren S, Yan XT, Li HP, Li W, Zheng B, et al. Improvement of Cisplatin-induced renal dysfunction by Schisandra chinensis stems via anti-inflammation and anti-apoptosis effects. Journal of ethnopharmacology. 2018;217:228-37.
41. Wang W, Zhou PH, Xu CG, Zhou XJ, Hu W, Zhang J. Baicalein attenuates renal fibrosis by inhibiting inflammation via down-regulating NF-kappaB and MAPK signal pathways. Journal of molecular histology. 2015;46(3):283-90.
42. Anders HJ, Suarez-Alvarez B, Grigorescu M, Foresto-Neto O, Steiger S, Desai J, et al. The macrophage phenotype and inflammasome component NLRP3 contributes to nephrocalcinosis-related chronic kidney disease independent from IL-1-mediated tissue injury. Kidney international. 2018;93(3):656-69.
43. Hao GH, Niu XL, Gao DF, Wei J, Wang NP. Agonists at PPAR-gamma suppress angiotensin II-induced production of plasminogen activator inhibitor-1 and extracellular matrix in rat cardiac fibroblasts. British journal of pharmacology. 2008;153(7):1409-19.
44. Chung S, Kim S, Son M, Kim M, Koh ES, Shin SJ, et al. Inhibition of p300/CBP-Associated Factor Attenuates Renal Tubulointerstitial Fibrosis through Modulation of NF-kB and Nrf2. International journal of molecular sciences. 2019;20(7).
45. Li A, Zhang X, Shu M, Wu M, Wang J, Zhang J, et al. Arctigenin suppresses renal interstitial fibrosis in a rat model of obstructive nephropathy. Phytomedicine : international journal of phytotherapy and phytopharmacology. 2017;30:28-41.
46. Ahn DS, Lee HJ, Hwang J, Han H, Kim B, Shim B, et al. Lambertianic Acid Sensitizes Non-Small Cell Lung Cancers to TRAIL-Induced Apoptosis via Inhibition of XIAP/NF-kappaB and Activation of Caspases and Death Receptor 4. International journal of molecular sciences. 2018;19(5).

47. Lee HL, Kang KS. Protective effect of ginsenoside Rh3 against anticancer drug-induced apoptosis in LLC-PK1 kidney cells. Journal of ginseng research. 2017;41(2):227-31.
48. Yang WZ, Zhou H, Yan Y. XIAP underlies apoptosis resistance of renal cell carcinoma cells. Molecular medicine reports. 2018;17(1):125-30.
49. Atabai K, Fernandez R, Huang X, Ueki I, Kline A, Li Y, et al. Mfge8 is critical for mammary gland remodeling during involution. Molecular biology of the cell. 2005;16(12):5528-37.
50. Miksa M, Wu R, Dong W, Komura H, Amin D, Ji Y, et al. Immature dendritic cell-derived exosomes rescue septic animals via milk fat globule epidermal growth factor-factor VIII [corrected]. Journal of immunology (Baltimore, Md : 1950). 2009;183(9):5983-90.
51. Cen C, Aziz M, Yang WL, Zhou M, Nicastro JM, Coppa GF, et al. Milk fat globule-epidermal growth factor-factor VIII attenuates sepsis-induced acute kidney injury. The Journal of surgical research. 2017;213:281-9.
52. Li H, Zhang T, Wang K, Lu M, Guo Y, Zhang Y, et al. MFGE8 protects against CCl4 -induced liver injury by reducing apoptosis and promoting proliferation of hepatocytes. Journal of cellular physiology. 2019.
53. Liu F, Chen Y, Hu Q, Li B, Tang J, He Y, et al. MFGE8/Integrin beta3 pathway alleviates apoptosis and inflammation in early brain injury after subarachnoid hemorrhage in rats. Experimental neurology. 2015;272:120-7.

Figures

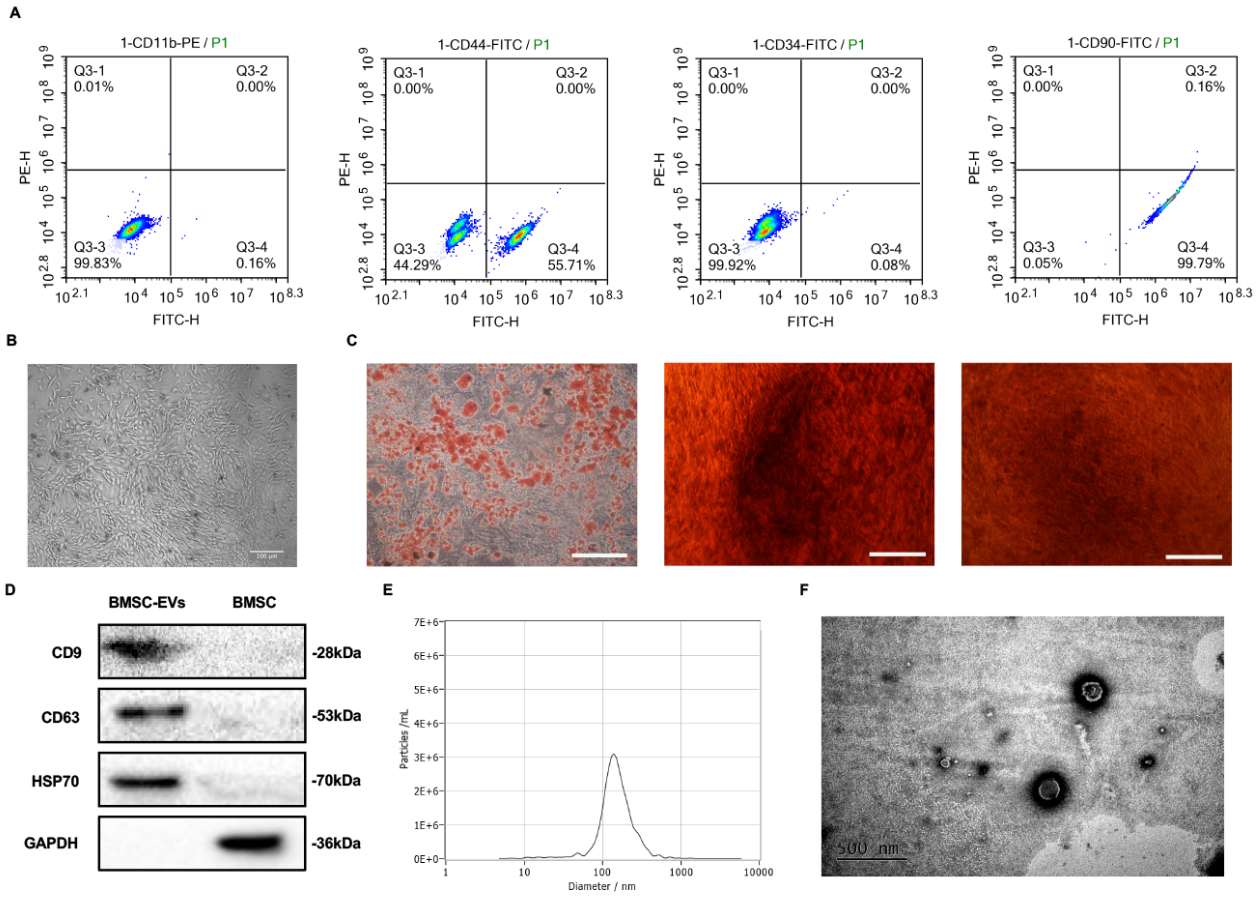

Figure 1

Characterization of BMSCs and BMSCs derived extracellular vesicles. A Flow cytometric analysis for detection of BMSCs surface markers. B Morphology of BMSCs. Scale bar: 100μm. C Adipogenic, chondrogenic, and osteogenic differentiation potentials of BMSCs. Scale bar: 100μm. D Western blot was used to confirm the expression of EVs specific markers CD9, CD63, and HSP70. E Particle size distribution. F Representative transmission electron microscopy image of BMSC-EVs, showing a typical spheroid shape. Scale bar: 500nm.

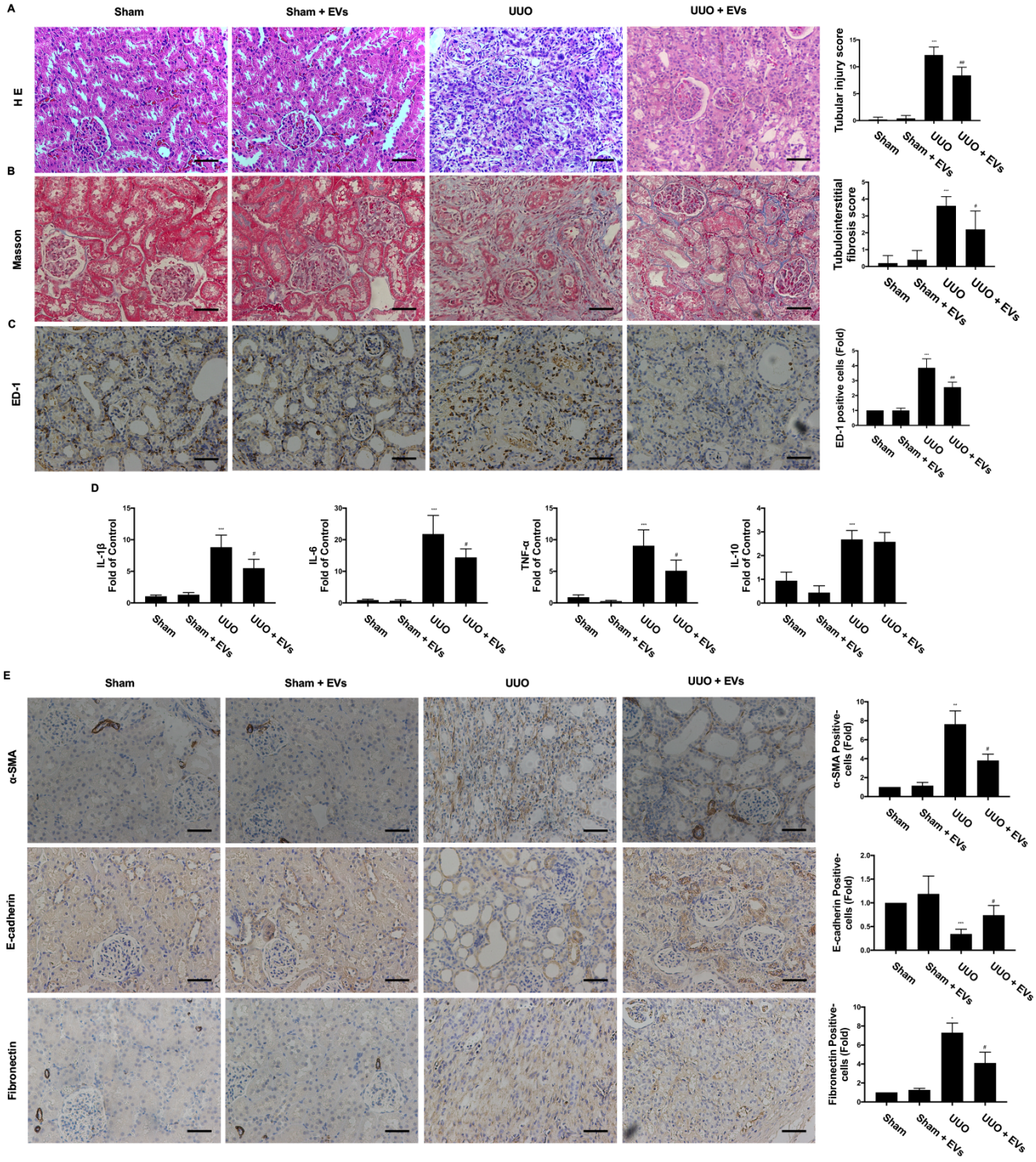

Figure 2

Effects of BMSC-EVs on the tubular damage, collagen deposition, fibrosis, and inflammation in UUO kidneys. A Representative image of the HE staining from kidneys of Sham, Sham + BMSC-EVs, UUO, UUO + BMSC-EVs rats, bar graph depicts tubular injury scores based on HE staining. Scale bar: 100μm. B Representative image of Masson's trichrome staining from kidneys of Sham, Sham + BMSC-EVs, UUO, UUO + BMSC-EVs rats, bar graph depicts renal interstitial fibrosis scores based on Masson's trichrome

staining. Scale bar: 100μm. C Representative images illustrating infiltration of ED-1-postive macrophages of rat kidneys in different groups, quantification of the number of ED-1-postive macrophages pre field in different groups. Scale bar: 150μm. D RT-PCR analysis of gene expression was performed for inflammatory mediators IL-1β, IL-6, TNF-α, and IL-10. E The locations and expressions of α-SMA, E-cadherin, and Fibronectin were determined by immunohistochemical staining in the kidney sections of rats from different groups, semi-quantitative immunohistochemical analysis of the EMT-related protein expression in different groups. Scale bar: 100μm. *P<0.05, **P<0.01, ***P<0.001 (compared with Sham group); #P<0.05, ##P<0.01, ###P<0.001 (compared with UUO group).

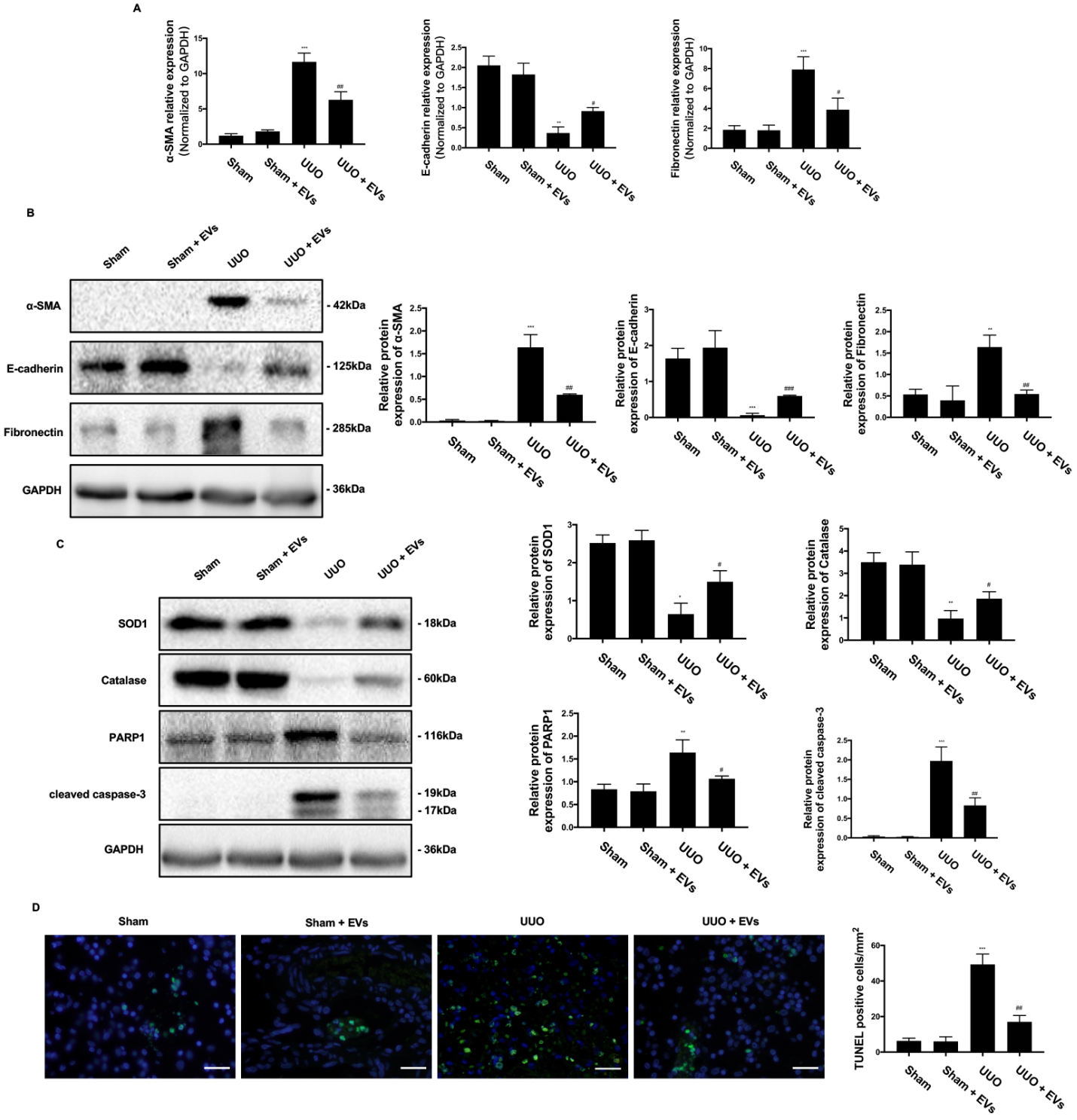

Figure 3

Effects of BMSC-EVs on the EMT process, oxidative stress and cell apoptosis in UUO kidneys. A The mRNA levels of α-SMA, E-cadherin, and Fibronectin were detected by RT-PCR. B The protein expressions for α-SMA, E-cadherin, and Fibronectin were detected by Western blot, and the protein levels of α-SMA, E-cadherin, and Fibronectin were expressed as arbitrary densitometric units and normalized by the value of GAPDH. C The protein expressions for SOD1, Catalase, PARP1 and cleaved caspase-3 were detected by

Western blot. and the protein levels of SOD1, Catalase, PARP1 and cleaved caspase-3 were expressed as arbitrary densitometric units and normalized by the value of GAPDH. D Representative images of rat kidneys of different groups by TUNEL staining and TUNEL positive cells counted in kidneys. Scale bar: 50μm. *P<0.05, **P<0.01, ***P<0.001 (compared with Sham group); #P<0.05, ##P<0.01, ###P<0.001 (compared with UUO group).

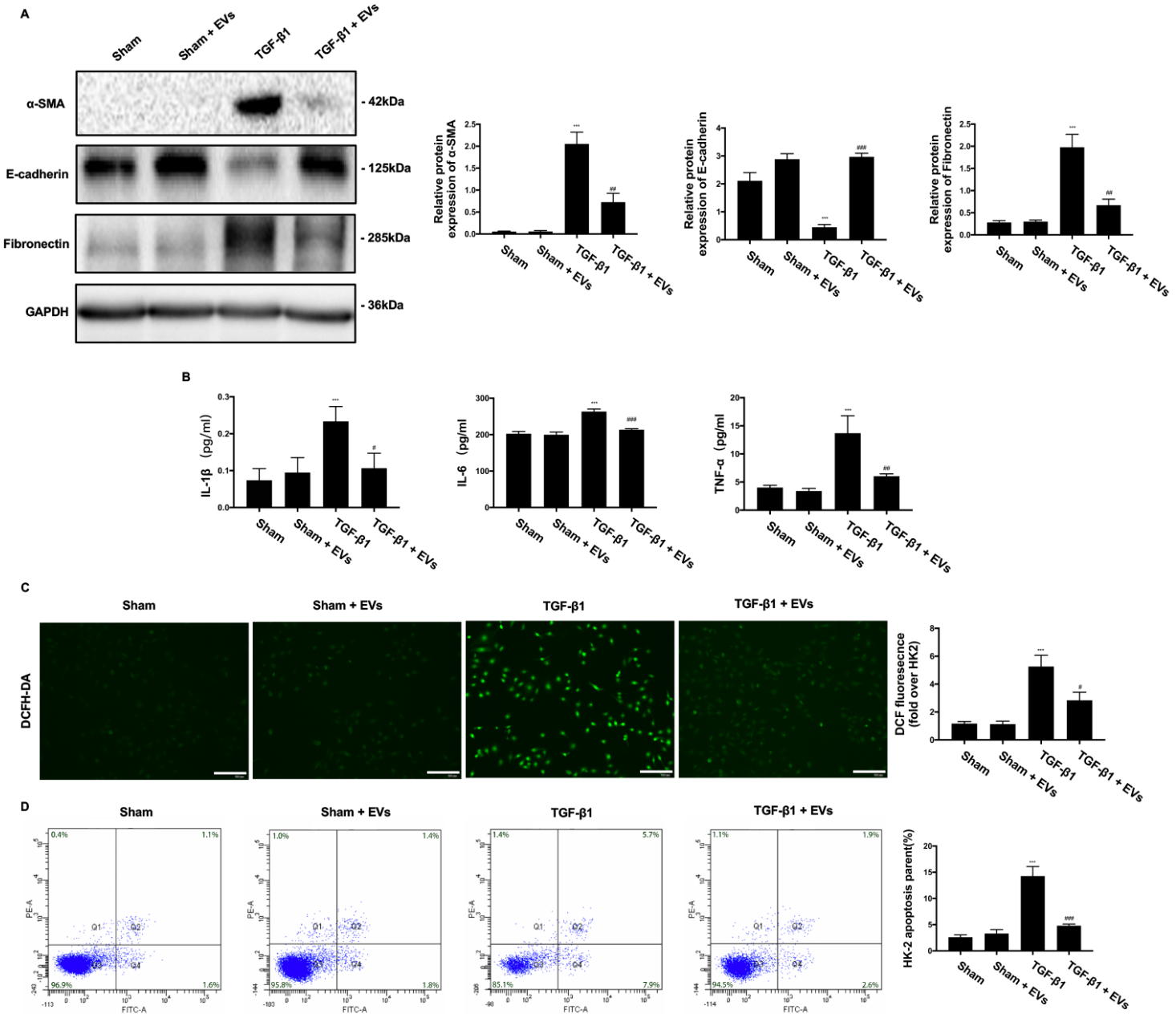

Figure 4

Effects of BMSC-EVs on TGF-β1-induced EMT process, inflammation, oxidative stress and apoptosis in HK-2 cells. A The protein expressions for α-SMA, E-cadherin, and Fibronectin were detected by Western blot, and the protein levels of α-SMA, E-cadherin, and Fibronectin were expressed as arbitrary densitometric units and normalized by the value of GAPDH. B The levels of IL-1β, IL-6, and TNF-α were

detected with ELISA kits. C Representative image of HK-2 cells stained with 2’7’-dichlorodihydrofluorescein diacetate (DCFH-DA). Quantification of DCFH-DA . Scale bar: 100μm. D Rate of cell apoptosis as qualified by flow cytometry. *P<0.05, **P<0.01, ***P<0.001 (compared with Sham group); #P<0.05, ##P<0.01, ###P<0.001 (compared with TGF-β1 group).

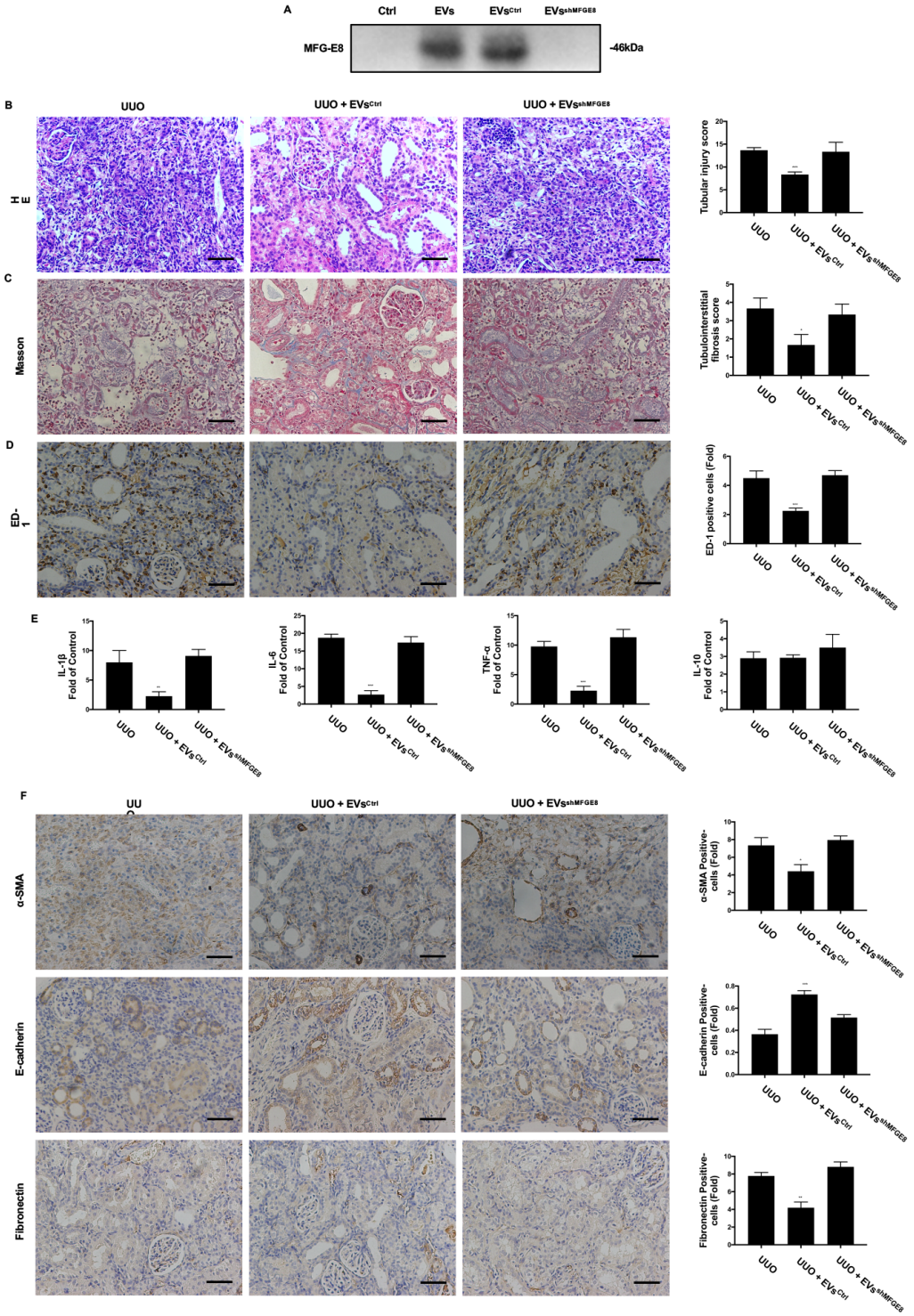

Figure 5

Effect of MFGE8-silenced EVs on tubular damage, collagen deposition, fibrosis, and inflammation in UUO kidneys. A A representative Western blot showing the secretion of MFG-E8 from Control, BMSC-EVs, BMSC-EVsCtrl, and BMSC-EVsshMFGE8. B Representative image of the HE staining from kidneys of UUO, UUO + EVsCtrl, and UUO + EVsshMFGE8 rats, bar graph depicts tubular injury scores based on HE staining. Scale bar: 100μm. C Representative image of Masson's trichrome staining from kidneys of UUO, UUO + EVsCtrl, and UUO + EVsshMFGE8 rats, bar graph depicts renal interstitial fibrosis scores based on Masson's trichrome staining. Scale bar: 100μm. D Representative images illustrating infiltration of ED-1-postive macrophages of rat kidneys in different groups, quantification of the number of ED-1-postive macrophages pre field in different groups. Scale bar: 150μm. E RT-PCR analysis of gene expression was performed for inflammatory mediators IL-1β, IL-6, TNF-α, and IL-10. F The locations and expressions of α-SMA, E-cadherin, and Fibronectin were determined by immunohistochemical staining in the kidney sections of rats from different groups, semi-quantitative immunohistochemical analysis of the EMT-related protein expression in different groups. Scale bar: 100μm. *P<0.05, **P<0.01, ***P<0.001 (compared with Sham group); #P<0.05, ##P<0.01, ###P<0.001 (compared with UUO group).

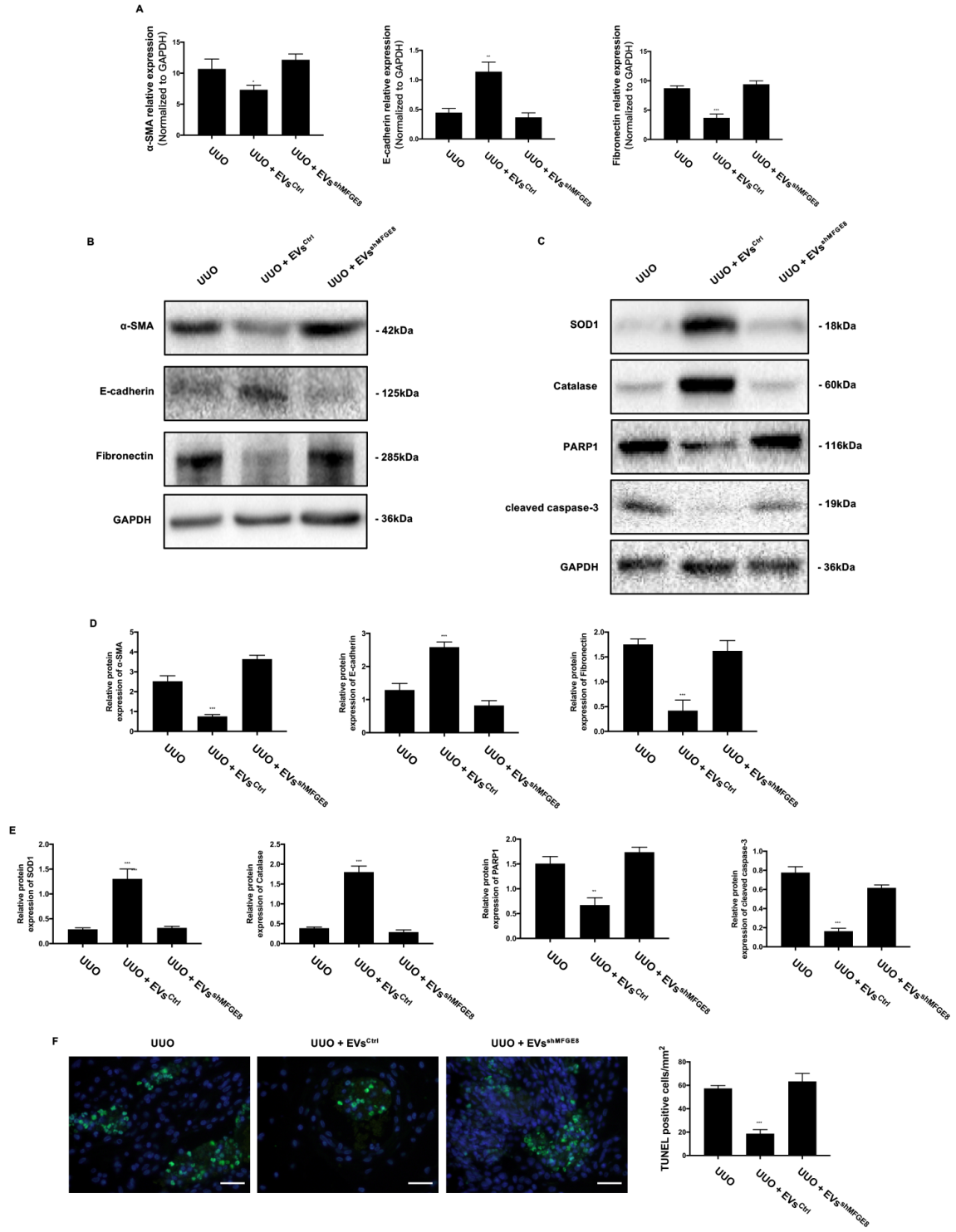

Figure 6

Effects of MFGE8-silenced EVs on the EMT process, oxidative stress and apoptosis in UUO kidneys. A The mRNA levels of α-SMA, E-cadherin, and Fibronectin were detected by RT-PCR. B, D The protein expressions for α-SMA, E-cadherin, and Fibronectin were detected by Western blot, and the protein levels of α-SMA, E-cadherin, and Fibronectin were expressed as arbitrary densitometric units and normalized by the value of GAPDH. C, E The protein expressions for SOD1, Catalase, PARP1 and cleaved caspase-3 were

detected by Western blot. and the protein levels of SOD1, Catalase, PARP1 and cleaved caspase-3 were expressed as arbitrary densitometric units and normalized by the value of GAPDH. F Representative images of rat kidneys of different groups by TUNEL staining and TUNEL positive cells counted in kidneys. Scale bar: 50μm. *P<0.05, **P<0.01, ***P<0.001 (compared with UUO group).

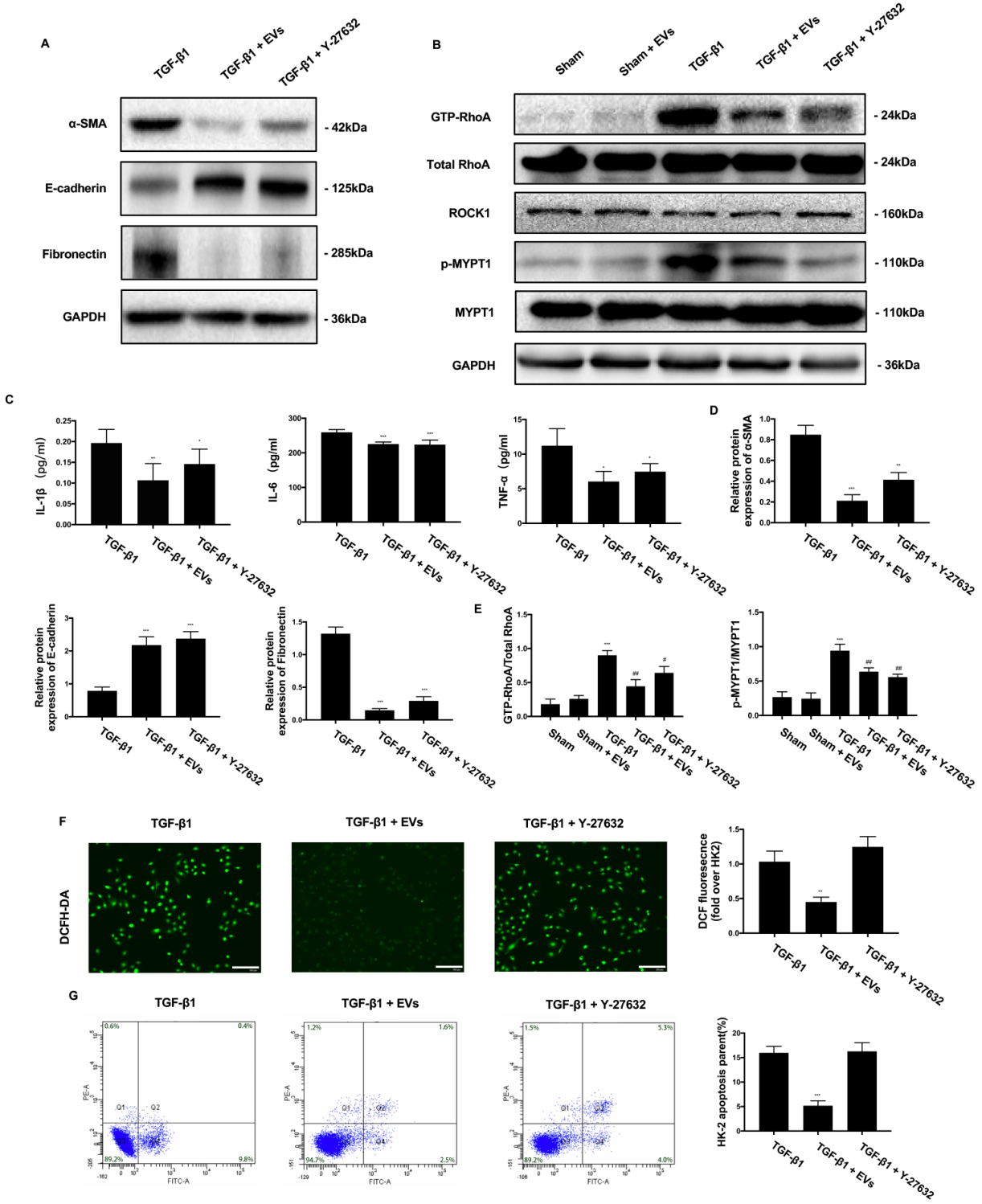

Figure 7

BMSC-EVs deliver nephroprotection via partly inhibiting the RhoA/ROCK pathway. A, D The protein expressions for α-SMA, E-cadherin, and Fibronectin were detected by Western blot, and the protein levels of α-SMA, E-cadherin, and Fibronectin were expressed as arbitrary densitometric units and normalized by the value of GAPDH. B, E The protein expressions for GTP-RhoA, total RhoA, ROCK1, p-MYPT1 and MYPT1 were detected by Western blot. C The levels of IL-1β, IL-6, and TNF-α were detected with ELISA kits. F Representative image of HK-2 cells stained with 2′7′-dichlorodihydrofluorescein diacetate (DCFH-DA). Quantification of DCFH-DA. Scale bar: 100μm. G Rate of cell apoptosis as qualified by flow cytometry. *P<0.05, **P<0.01, ***P<0.001 (compared with Sham group); #P<0.05, ##P<0.01, ###P<0.001 (compared with TGF-β1 group).